RL-TR-97-152
In-House Report
July 1997

ELECTRON DENSITY AND TEMPERATURE DURING THE CHARGE-2B SOUNDING ROCKET MISSION

James Ernstmeyer, Timothy J. Tanigawa and Neil B. Myers

APPROVED FOR PUBLIC RELEASE; DISTRIBUTION UNLIMITED.

Rome Laboratory
Air Force Materiel Command
Rome, New York

This report has been reviewed by the Rome Laboratory Public Affairs Office (PA) and is releasable to the National Technical Information Service (NTIS). At NTIS it will be releasable to the general public, including foreign nations.

RL-TR-97-152 has been reviewed and is approved for publication.

APPROVED: Robert V. McGahan

ROBERT V. McGAHAN
Chief, Applied Electromagnetics Division
Electromagnetics & Reliability Directorate

FOR THE COMMANDER:

HORST R. WITTMANN, Director
Electromagnetics & Reliability Directorate

If your address has changed or if you wish to be removed from the Rome Laboratory mailing list, or if the addressee is no longer employed by your organization, please notify Rome Laboratory/ERCP, Hanscom AFB, MA 01731. This will assist us in maintaining a current mailing list.

Do not return copies of this report unless contractual obligations or notices on a specific document require that it be returned.

REPORT DOCUMENTATION PAGE

Form Approved
OMB No. 0704-0188

1. AGENCY USE ONLY *(Leave blank)*	2. REPORT DATE	3. REPORT TYPE AND DATES COVERED
	JULY 1997	IN-HOUSE

4. TITLE AND SUBTITLE
ELECTRON DENSITY AND TEMPERATURE DURING THE CHARGE-2B SOUNDING ROCKET MISSION

5. FUNDING NUMBERS
PE - 61102F
PR - 2304
TA - I2
WU - 02

6. AUTHOR(S)
James Ernstmeyer, Timothy J. Tanigawa and Neil B. Myers

7. PERFORMING ORGANIZATION NAME(S) AND ADDRESS(ES)
Rome Laboratory/ERCP
31 Grenier Street
Hanscom AFB, MA 01731-3010

8. PERFORMING ORGANIZATION REPORT NUMBER
RL-TR-97-152

9. SPONSORING/MONITORING AGENCY NAME(S) AND ADDRESS(ES)
Rome Laboratory/ERCP
31 Grenier Street
Hanscom AFB, MA 01731-3010

10. SPONSORING/MONITORING AGENCY REPORT NUMBER

11. SUPPLEMENTARY NOTES
Rome Laboratory Project Engineer: James Ernstmeyer, RL/ERCP, (617) 377-8977

12a. DISTRIBUTION AVAILABILITY STATEMENT
Approved for Public Release; Distribution Unlimited.

12b. DISTRIBUTION CODE

13. ABSTRACT *(Maximum 200 words)*
The CHARGE-2B sounding rocket was launched from Poker Flats Research Range, Alaska, in March 1992 to investigate VLF electromagnetic radiation generated by a modulated electron beam in the ionosphere. A Langmuir probe on board the Rome Laboratory Diagnostic Free Flyer (DFF) subpayload was the only source of local electron density and temperature data for the mission. The probe detected supra-thermal electrons generated by the beam injections. These observations were used to characterize the disturbed plasma region surrounding the beam-vehicle system. Spectral analysis of the probe current data reveals a low level of electron density fluctuation despite clear signatures of electrostatic beam emissions on the DFF wave observations.

14. SUBJECT TERMS
Langmuir probe, Active experiments, Electron beams, Ionospheric electron density

15. NUMBER OF PAGES
30

16. PRICE CODE

17. SECURITY CLASSIFICATION OF REPORT	18. SECURITY CLASSIFICATION OF THIS PAGE	19. SECURITY CLASSIFICATION OF ABSTRACT	20. LIMITATION OF ABSTRACT
UNCLASSIFIED	UNCLASSIFIED	UNCLASSIFIED	U/L

Contents

Illustrations

Preface

Thanks to Mr. Carl P. Ferioli for his crucial role in designing and fabricating the CHARGE-2B Langmuir probe. This work was sponsored in part by the Air Force Office of Scientific Research, Bolling AFB, DC.

Electron Density and Temperature During the CHARGE-2B Sounding Rocket Mission

1. INTRODUCTION

The CHARGE-2B sounding rocket payload (NASA mission 39.003 Raitt) was launched from the Poker Flat Research Range, Chatanika, Alaska, at 2227 hours local time on 28 March 1992. Its mission was to establish the feasibility of using a modulated electron beam in the ionosphere to radiate very low frequency (3 to 30 kHz) electromagnetic waves for reception on the ground. An additional objective not discussed in this report was to study the fluctuating and steady-state dynamics of an electron beam-spacecraft system immersed in the ionospheric plasma. A general description of the payload and some preliminary results were reported by Raitt.[1]

The Diagnostic Free Flyer (DFF) was one of three autonomous subpayloads that flew as part of CHARGE-2B. The two other subpayloads, the Mother and the Daughter,

---

Received for publication 1 Aug 1997.

[1] Raitt, W.J., Ernstmeyer, J., Myers, N.B., White, A.B., Sasaki, S., Oyama, K-I, Kawashima, N., Fraser-Smith, A.C., Gilchrist, B.E., and Hallinan, T.J. (1995) VLF wave experiments in space using a modulated electron beam, *J. Spacecraft and Rockets*, **32**:670-679.

were connected during the flight by an insulated, conducting wire. This configuration permitted the Daughter to act as a reference electrode for measuring the potential of the beam-emitting Mother payload relative to the background plasma. A discussion of this will be the subject of a future paper. The DFF made *in situ* wave observations during 3-kV, 2-A modulated beam emissions from the Mother. To this end, it carried electric and magnetic wave detectors as well as a Langmuir probe. Unlike the Daughter, the DFF was untethered. It separated from the Mother at a speed of 5.3 m/s and an inclination of 6° to the geomagnetic field. The DFF was spin stabilized at a spin rate of 1.105 rotations per second. Along with the other subpayloads, the DFF reached an apogee of 266 km during the flight. The trajectory of the payload is shown in Figure 1.

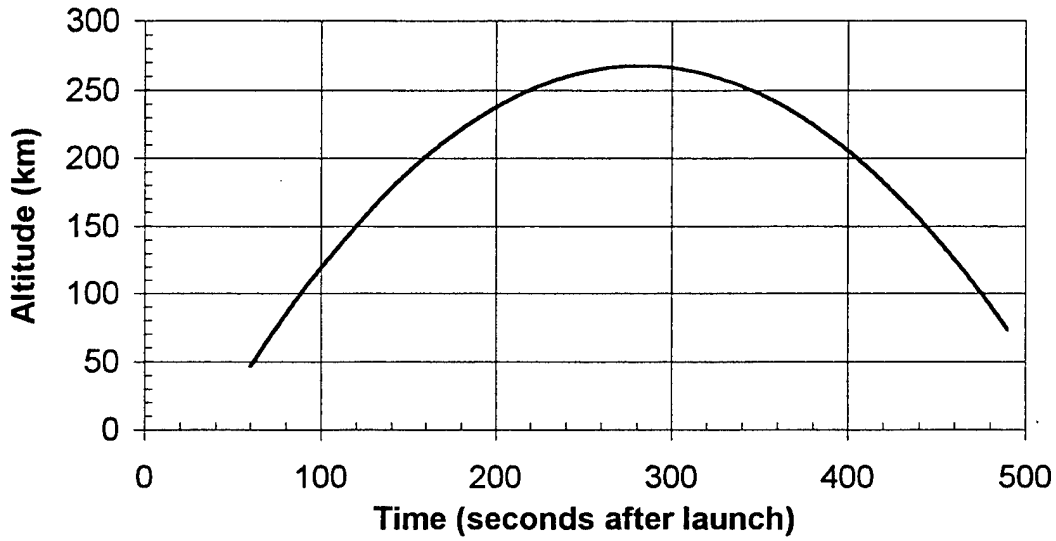

Figure 1. Trajectory of the CHARGE-2B payload.

The Langmuir probe on board the DFF provided the only measurements of the ambient electron densities and temperatures encountered by the payload during the flight. The probe results therefore played several crucial roles in the wave data analysis. First, electron density is a key parameter defining the VLF dispersion properties of the local plasma.[2] This has been discussed in a separate paper[3]. Second, electron temperature observations determine the character and size of the disturbed plasma region surrounding the Mother. Finally, since CHARGE-2B was launched under conditions of weak diffuse aurora,[4] the observed electron density-altitude profile differed dramatically from typical

---

[2] Helliwell, R.A. (1965) *Whistlers and Related Ionospheric Phenomena*, Stanford University Press, Stanford.

[3] Schriver, D., Sotnikov, V.I., Ashour-Abdalla, M., and Ernstmeyer, J., Propagation of beam-driven VLF waves from the ionosphere toward the ground, *Journal of Geophysical Research*, **100**: 3693-3702.

[4] Hallinan, T.J. (1993) *Video Imaging of CHARGE IIB Auroral Streaks*, RL-TR-93-242, Final Report, Contract F19628-91-K-0035, University of Alaska, Fairbanks.

modeled profiles, as discussed in Section 5. As a result, analysis of the wave data would have been difficult in the absence of the Langmuir probe results.

In light of the importance of the Langmuir probe to future analysis of the CHARGE-2B data, we will document the flight configuration of the instrument and its essential results in this report. In Section 2 we will describe the physical characteristics of the probe, along with the governing equations and assumptions employed in the reduction of the probe data. In Section 3, we will present time and altitude profiles of the reduced plasma parameters. In the subsequent sections we will present observations of the heated plasma and density fluctuations.

2. LANGMUIR PROBE CHARACTERISTICS

Figure 2 shows the Langmuir probe flown on CHARGE-2B. It evolved from a similar probe flown on the Phillips Laboratory (then Air Force Geophysics Laboratory) BERT sounding rocket mission.[5] In the transition, the probe collecting area was reduced by a factor of 4 and the construction was simplified to facilitate in-house assembly of the sensor. The reduction in probe collecting area was undertaken to counter the tendency of positive probe bias to swing the host spacecraft potential negative with respect to the background plasma. This effect results from the great disparity between electron and ion mobility, and may be avoided by minimizing the ratio of probe surface area to vehicle-plasma contact area. For the DFF, the computed value of this ratio was 0.7%, which was below the acceptable upper limit of 1%.[6] Nevertheless, floating probe measurements in Figure 3 show evidence of the Langmuir probe biasing the vehicle skin. The negative peak in the measured skin potential at 178.5 s was due to the sweep voltage applied to the Langmuir probe. This bias of the skin potential by the probe sweep voltage may have been due to surface oxidation of the payload skin insulating the payload ground from the ambient plasma.

The Langmuir probe on the DFF was of the spherical, gridded variety. The diameter of the grid was 2.54 cm, and that of the solid center conductor, 1.68 cm. As illustrated in Figure 3, the grid potential with respect to the DFF skin was swept linearly from -3 V to +5 V and back in one second, then held at +3 V for 1 second, and finally held at 0 V for 2 seconds. The swept bias segments were used to obtain the plasma current-voltage characteristic, the constant bias segment provided data on plasma density fluctuations, and the zero bias segment assured that there would be times when the payload skin potential could not be influenced by the Langmuir probe. This sweep program was maintained throughout the flight. At all times, the center collector was maintained at a +20 V potential with respect to the grid in order to prevent ion collection,

---

[5] Ernstmeyer, J., and Donatelli, D.E. (1990) Vehicle charging and associated HF wave phenomena during electron beam emissions, *Radio Science,* **25**:263-275.

[6] Boyd, R.L.F. (1968) Langmuir probes on spacecraft, in *Plasma Diagnostics,* Lochte-Holtgreven, Ed., John Wiley and Sons, New York.

to suppress secondary electron emission, and to ensure that all electrons passing through the grid were, in fact, collected. Effective transparency of the grid was estimated at 80 % due to the ratio of the size of the spaces to the size of the wire of the grid.

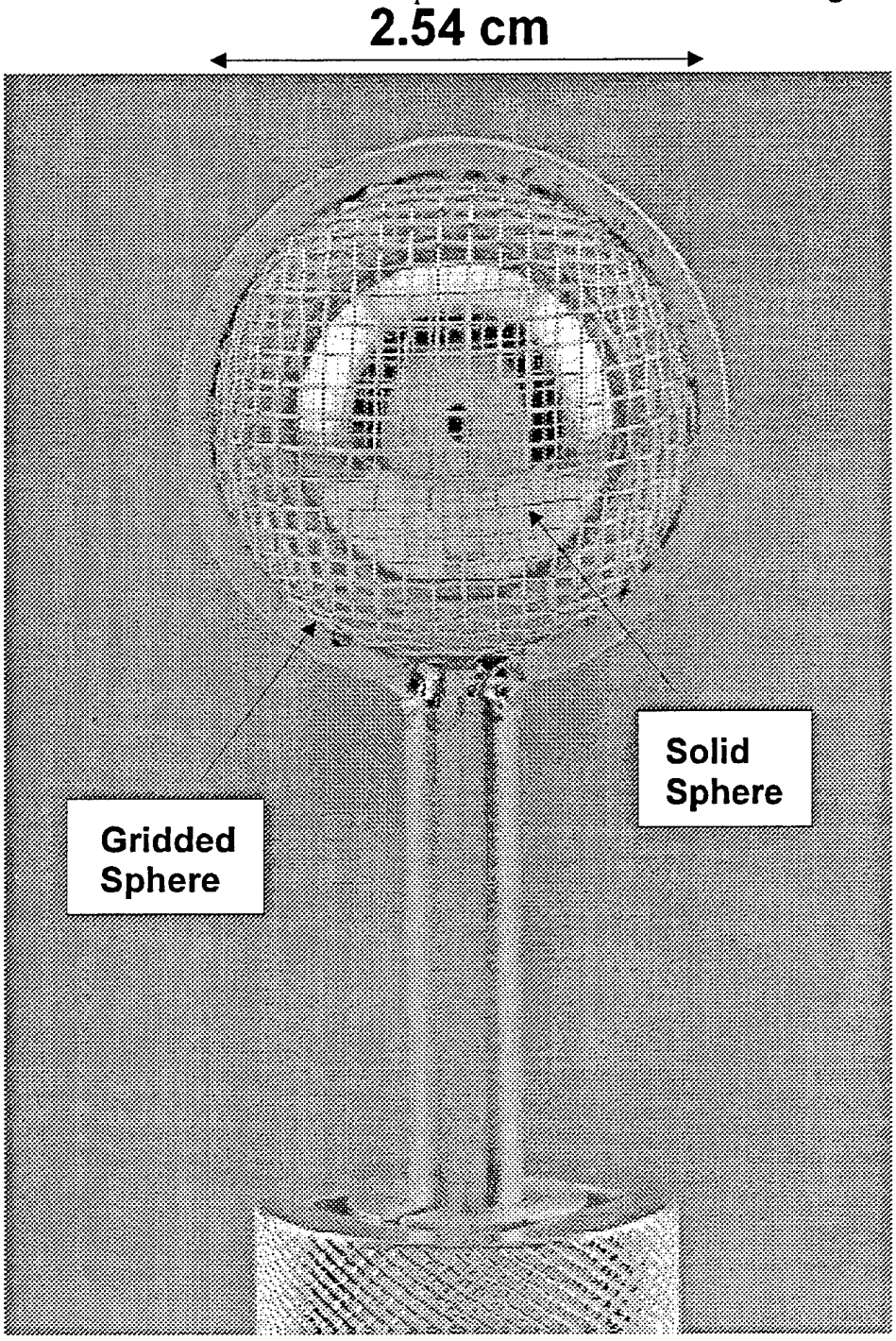

Figure 2. Langmuir Probe Gridded Sphere and Dimensions.

In order to establish the highest electron temperature for which the probe will provide accurate results, one must compute the electrostatic field between the grid and

center collector. This is readily accomplished for the ideal case. From this result, we obtain the temperature T_{max} of the most energetic electron that is certain to be trapped by the probe.

$$T_{max} = \frac{\Phi}{2\left(\frac{r_0}{r_1} - 1\right)} \tag{1}$$

where Φ is the grid to collector potential in volts, r_0 is the grid radius, r_1 is the collector radius, and T_{max} is in electron volts. For the geometry employed in the DFF Langmuir probe, T_{max} is 19.5 eV.

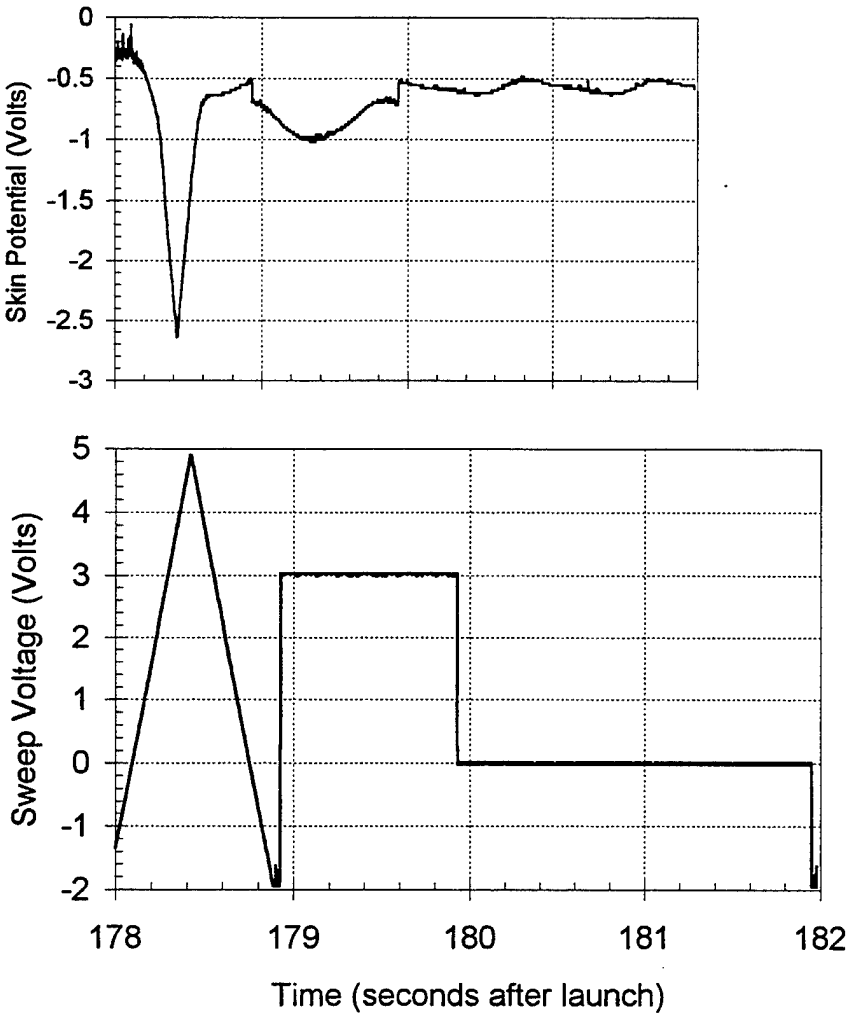

Figure 3. DFF Vehicle Potential Influenced by the Langmuir Probe. Upper frame shows the DFF skin potential measured with respect to a spherical floating probe deployed on an insulating boom. Bottom frame illustrates the Langmuir probe grid bias with respect to the DFF skin.

Currents collected by the probe were measured using a floating logarithmic electrometer adapted from the Phillips Lab BERT program. The resulting probe current signal was digitized at a rate of 5000 samples per second by the telemetry system. This channel was used during periods of fixed probe bias to investigate the electron density fluctuations characteristic of ELF electrostatic plasma oscillations. In addition, the sweeps were analyzed in the conventional manner to obtain electron density and temperature. Probe current sensitivity was 60 pA, and saturation was 100 μA. Probe bias was independently monitored on a companion channel digitized at 625 samples per second. The calibrations for the probe current and bias monitor channels are given below:

$$\log(i) = 1.25 \cdot (V_{tm} - 0.967) - 9.0 \tag{2}$$

$$V_{sweep} = 1.616 \cdot (V_{tm} - 1.149) \tag{3}$$

where probe current i is in amperes, bias voltage V_{sweep} is in volts, and telemetry voltage V_{tm} is in volts.

The Langmuir probe was deployed in the spin plane at a distance of 40.6 cm from the DFF spin axis. The probe was magnetically shadowed by the aft end of the DFF payload skin for as much as 10 degrees of payload rotation out of every complete rotation. Some slight effects of this shadowing were observed at positive probe bias potentials.

3. REDUCTION OF SWEEP DATA

Data from the probe current channel taken during periods of swept probe bias provide the current-voltage characteristic of a sphere with the same diameter as the grid. Figure 4 shows an actual probe sweep divided into its three characteristic segments. The first is the retarding sweep, during which negative probe potentials retard the approach of all electrons and prevent a varying fraction of the electron population from arriving at the grid. The next segment is saturation, a brief period during which the probe is at or very close to plasma potential and no electrons are retarded. The final segment is the accelerating sweep, during which the grid is placed at positive potentials with respect to the plasma, creating a sheath around the probe and increasing the effective grid area. The amount of current collection increases with the effective grid area.

The division of the current-voltage characteristic into retarding, saturating, and accelerating segments is only indirectly related to the nominal applied voltage on the grid. The nominal applied bias is measured with respect to the payload skin. The voltage that matters for current collection, on the other hand, is measured with respect to the background plasma itself. The two voltages differ by the potential of the payload with respect to the background plasma, known as the floating potential. The floating potential is typically on the order of -1V and results from the differing mobility of the plasma electron and ion components. It varies with the plasma temperature and was not directly measured during the CHARGE-2B flight.

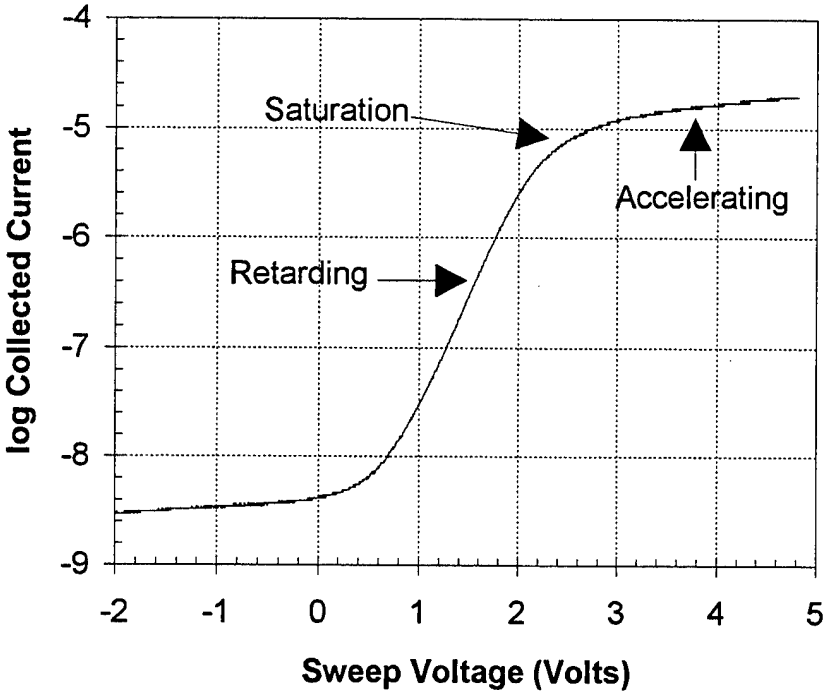

Figure 4. Langmuir Probe Current-Voltage Characteristic. This plot of probe current versus grid bias was obtained for the sweep starting 303.138 seconds after launch. For grid potentials below the plasma potential, the sweep is retarding; above the plasma potential, the sweep is accelerating. The point at which grid potential equals plasma potential is denoted as saturation.

Regardless of the value of the vehicle floating potential, we can identify the retarding sweep and saturation by inspection from plots such as Figure 5. If one then assumes an unmagnetized electron population in thermal equilibrium with its surroundings, the temperature and density of the plasma can be derived from the slope of the retarding sweep and the value of the saturation current, as follows.

We are assuming a system in thermal equilibrium, so the velocity distribution of the electrons will be Maxwellian. In that case, the current collected by the Langmuir probe will be[7]

$$i = A_{eff} e n_p \frac{v_{av}}{4} \text{ , where } v_{av} = 2\sqrt{\frac{2kT_e}{\pi\, m}} \qquad (4)$$

[7] Chen, F. F. (1965) Electric probes, in *Plasma Diagnostic Techniques*, R.H. Huddleston and S.L. Leonard, Ed., Academic Press, New York.

The effective probe area, A_{eff}, is the geometric surface area of the grid times the 0.8 transparency factor. The electron density at the grid is n_p. The electron charge, mass, and Boltzmann constant, respectively are e, m, and k. The electron plasma temperature is T_e.

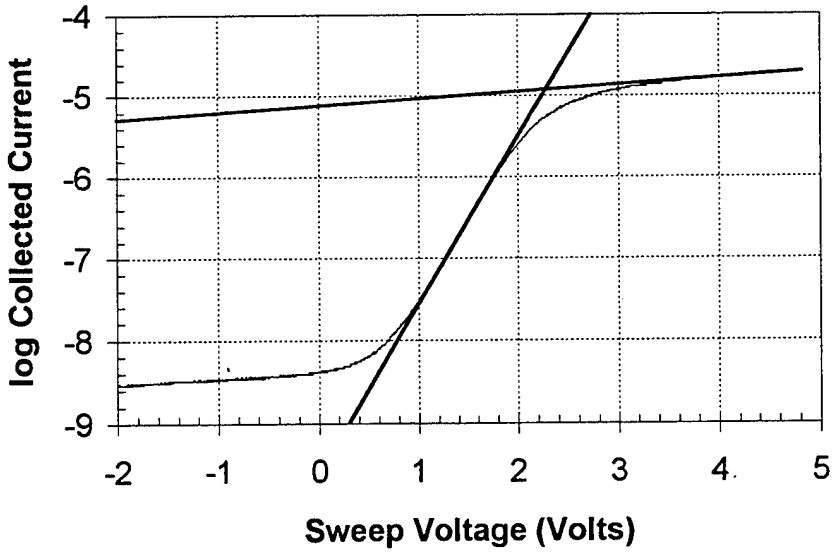

a)

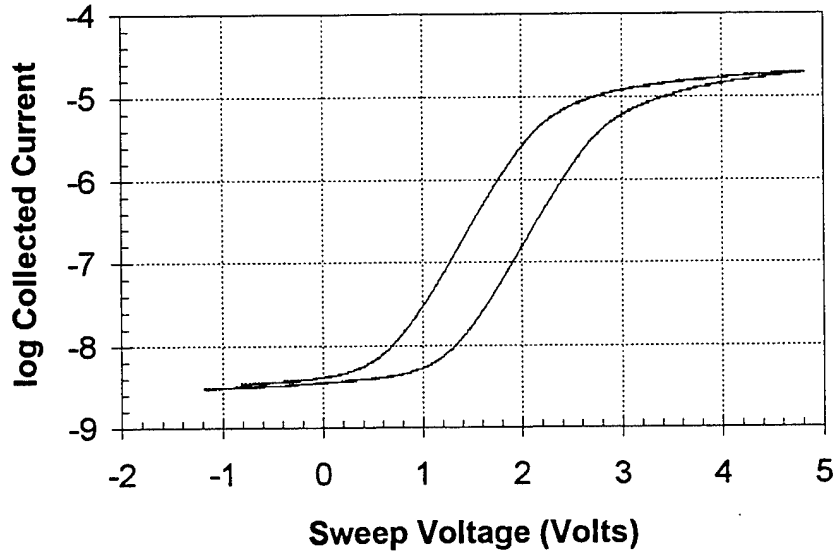

b)

Figure 5. a) Automated Reduction of Langmuir Probe Sweep Data. The data shown is from the sweep starting 303.138 seconds after launch. The construction line on the retarding sweep is tangent at the point of inflection. The construction line on the accelerating sweep is tangent at the point of maximum collected current. Saturation current is obtained from the intersection of the two lines. b) Hysteresis effect during the full voltage sweep.

The electron density at the grid is expressed using the Boltzmann factor as[7]

$$n_p = ne^{\frac{-eV}{kT_e}} \tag{5}$$

The grid potential appears here as V. The ambient electron density at large distances from the probe where $V = 0$, is denoted by n. Plasma density, n, and temperature, T_e, are the parameters we will derive. Substituting in the above expression for collected current i, we obtain

$$i = \frac{A_{eff}e}{2}\ n\,\mathrm{e}^{\frac{-eV}{kT_e}}\ \sqrt{\frac{2kT_e}{\pi\ m}} \tag{6}$$

To solve for an expression that yields the electron temperature we first take the logarithm of both sides.

$$\log(i) = \log\left(\frac{A_{eff}en}{2}\sqrt{\frac{2kT_e}{\pi\ m}}\right) - \frac{eV}{kT_e}\log(\mathrm{e}) \tag{7}$$

Differentiating with respect to voltage, substituting for the effective probe area and the various constants, and rearranging yields the electron temperature in electron Volts.

$$\frac{kT_e}{e} = \frac{-0.4343}{\frac{\mathrm{d}(\log(i))}{\mathrm{d}V}} \quad \text{(eV)} \tag{8}$$

The common practice is to plot the log of the current measurements versus the sweep voltage. Then d(log(i))/dV is determined from the slope at the retarding region, as discussed above and the electron temperature is determined from Eq. (8).

Using Eq. (6) we can derive an expression for the plasma density in terms of the electron temperature and current to the probe.

$$n = \frac{ie^{-\frac{3}{2}}\sqrt{2\pi\ m}}{A_{eff}\sqrt{\frac{kT_e}{e}}\ \mathrm{e}^{-\frac{eV}{kT_e}}} \tag{9}$$

The grid potential V is zero with respect to the background plasma at the saturation point of the graph, as discussed earlier. The saturation current i_{sat} is defined as the current at the intersection of the slopes of the retarding and accelerating regions shown in Figure 5. Substituting $V = 0$, i_{sat} for i, and the other constants into Eq. (9) yields an expression for

the background plasma density in terms of the saturation current, which is obtained from the measurement, and electron temperature, which is derived above.

$$n = 2.3 \times 10^{10} \frac{i_{sat}}{\sqrt{\frac{kT_e}{e}}} \quad (\text{cm}^{-3}) \tag{10}$$

An algorithm was developed to automatically extract the saturation current i_{sat} and retarding sweep slope from the recorded flight Langmuir probe current-voltage characteristics. This algorithm finds the inflection point of the retarding sweep characteristic and fits a straight line at that point to establish the slope. This line and another fitted to the accelerating portion of the curve are used in a geometrical construction to fix the location of the knee of the curve. The current at the knee is taken to be i_{sat}, as mentioned above. Figure 5a shows data from a representative sweep, together with the automated construction lines, to illustrate the typical high quality of the fits obtained.

A slight apparent hysteresis results from displacement current flowing into and out of the probe, shown in Figure 5b. Displacement current causes the measured electron current to be higher while the probe voltage is increasing, and lower while the probe voltage is decreasing. The dependence of the magnitude of the displacement current on probe voltage for a fixed sweep rate produces a uniform vertical offset between the upsweep and downsweep characteristics on a logarithmic plot. This artifact is removed from the data by averaging the temperature and density results from each pair of up and down sweeps.

4. BACKGROUND DENSITY AND TEMPERATURE MEASUREMENTS

All the Langmuir probe data from the flight were reduced to obtain electron density and temperature. A key objective was to estimate profiles for the undisturbed, ambient plasma through which any beam-generated VLF waves would propagate. However, we will see in the next section that during the portion of the flight in which the DFF was within 40 meters of the beam column, it was immersed in a heated plasma generated by electron gun operations on the Mother. During this period a multi-component electron population of more than one temperature surrounded the Langmuir probe, so that the assumption of thermal equilibrium was violated. An example of the output from the Langmuir probe while immersed in the hot plasma is shown in Figure 6. The top panel shows an elevated temperature measurement. The lower panel shows a plasma consisting of two components at different temperatures. The smaller slope between sweep voltages of -2 to +1 V yield a higher temperature than the larger slope between 1 and 3 V, as can be seen from Eq. (8). The automated data reduction scheme failed for these cases, and the resulting plasma parameters are not included in Figures 7 and 8.

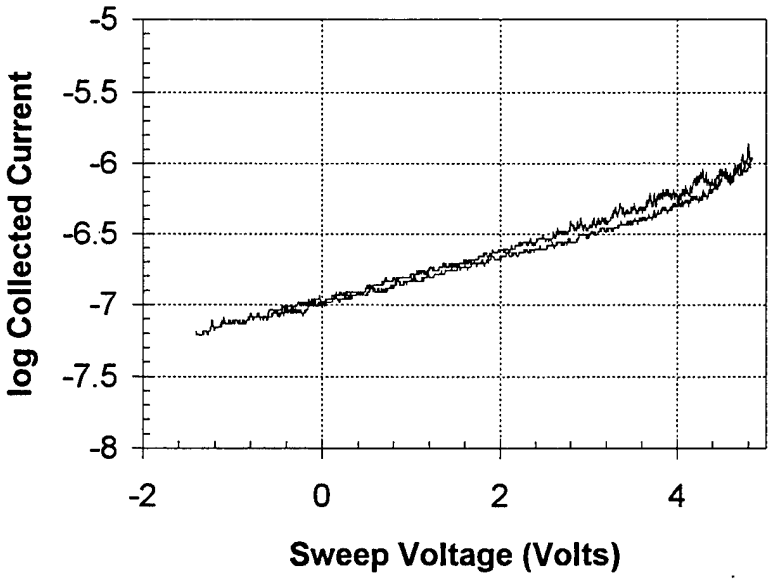

a)

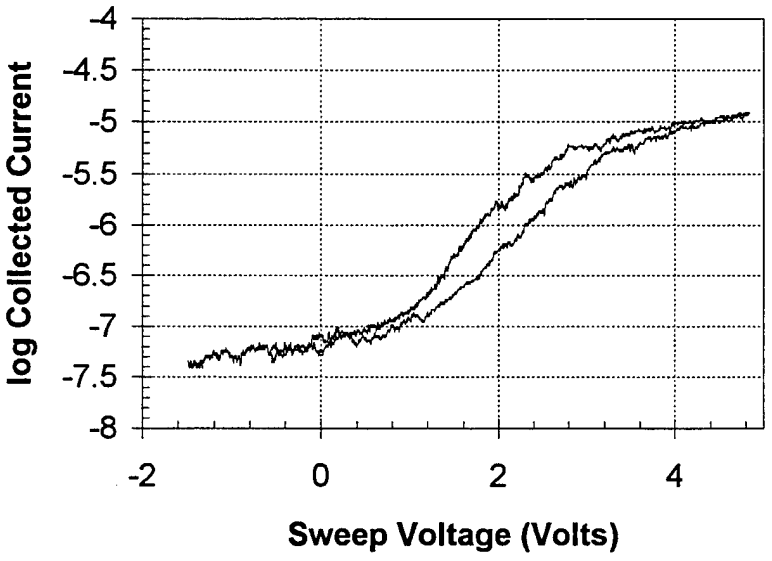

b)

Figure 6. Langmuir Probe Sweep Data in the Beam Heated Region Showing a) Elevated Electron Temperature, and b) a Two-Component Plasma.

Figure 7 shows electron density and temperature plotted against mission elapsed time in seconds after launch. The DFF was not deployed until 118.5 seconds after launch, accounting for the absence of Langmuir probe data until that time Figure 8 shows the same data plotted against altitude. The periods of the flight before and after apogee (the upleg and downleg, respectively) are distinguished by different symbols. Squares correspond to the upleg and triangles correspond to the downleg data.

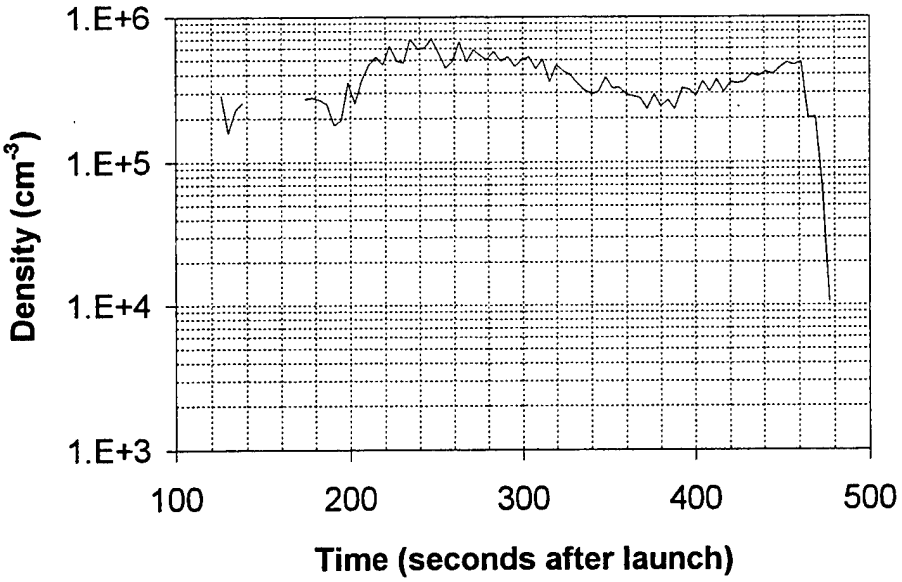

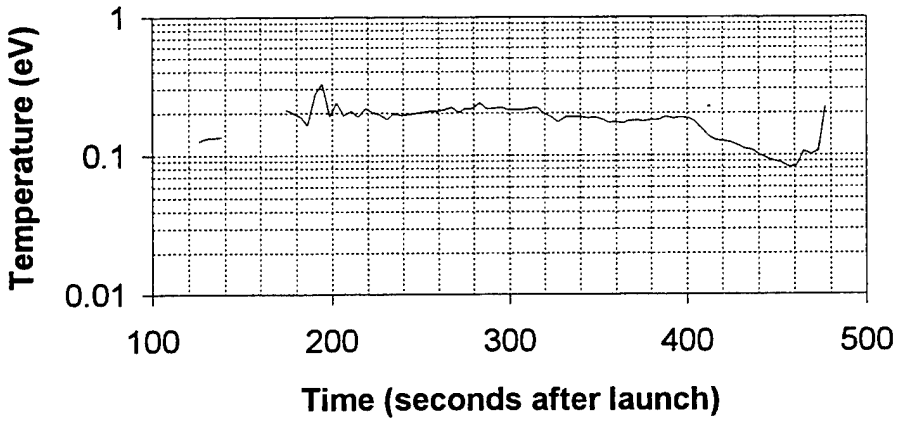

b)

Figure 7. a) Electron Density and b) Temperature Versus Mission Elapsed Time. Only data from the undisturbed plasma is plotted.

The measured densities and temperatures were for the most part well behaved, resulting from current-voltage characteristics similar to Figure 5. The low altitude portion of the profile, while thoroughly physical, is somewhat unexpected. Typical modeled nighttime profiles fall exponentially with decreasing altitude below 200 km. In the CHARGE-2B case, by contrast, electron densities remained elevated until 125 kilometers on the down leg. These relatively high electron densities are probably the result of auroral electron precipitation, also evidenced by weak, diffuse aurora observed from the ground during the mission.[4]

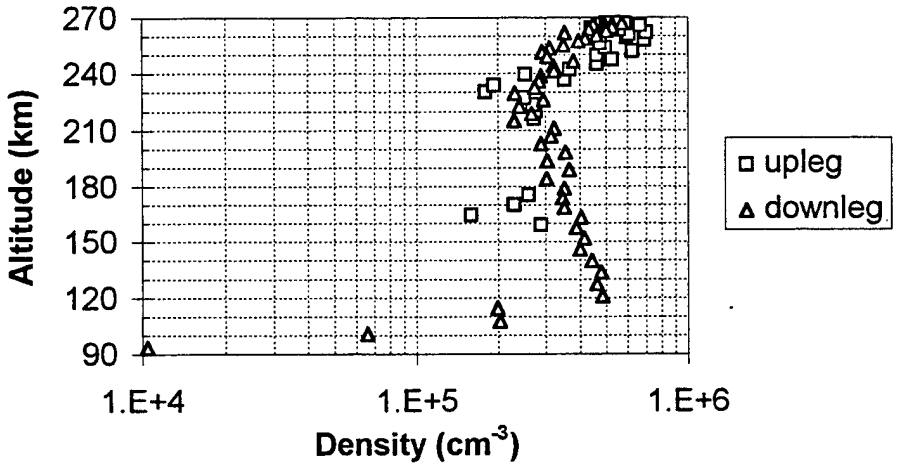

a)

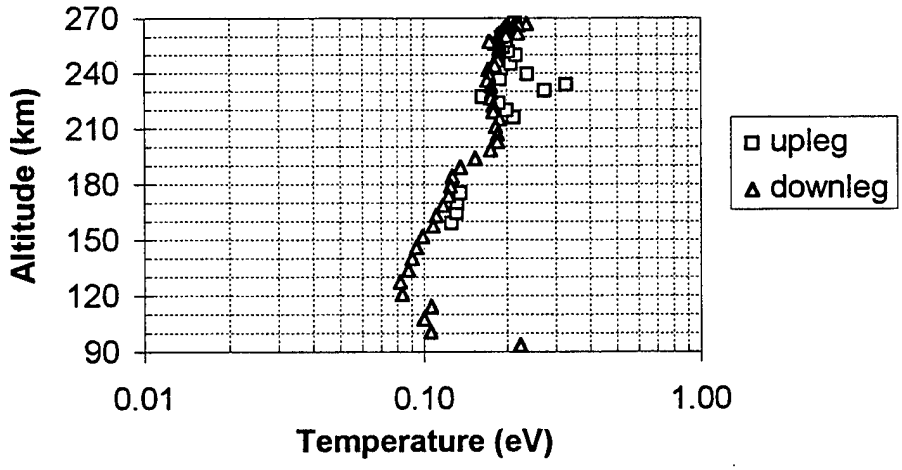

b)

Figure 8. a) Electron Density and b) Temperature Versus Altitude. Only data from the undisturbed plasma is plotted.

5. OBSERVATIONS OF THE HEATED PLASMA COLUMN

The DFF was deployed downward and nearly parallel to the geomagnetic field as shown in Figure 9. All of the beam operations at the beginning of the flight were directed downward. Thus, at the beginning of the flight the DFF was very near the electron beam because the beam is confined to spiral around the Earth's magnetic field lines.

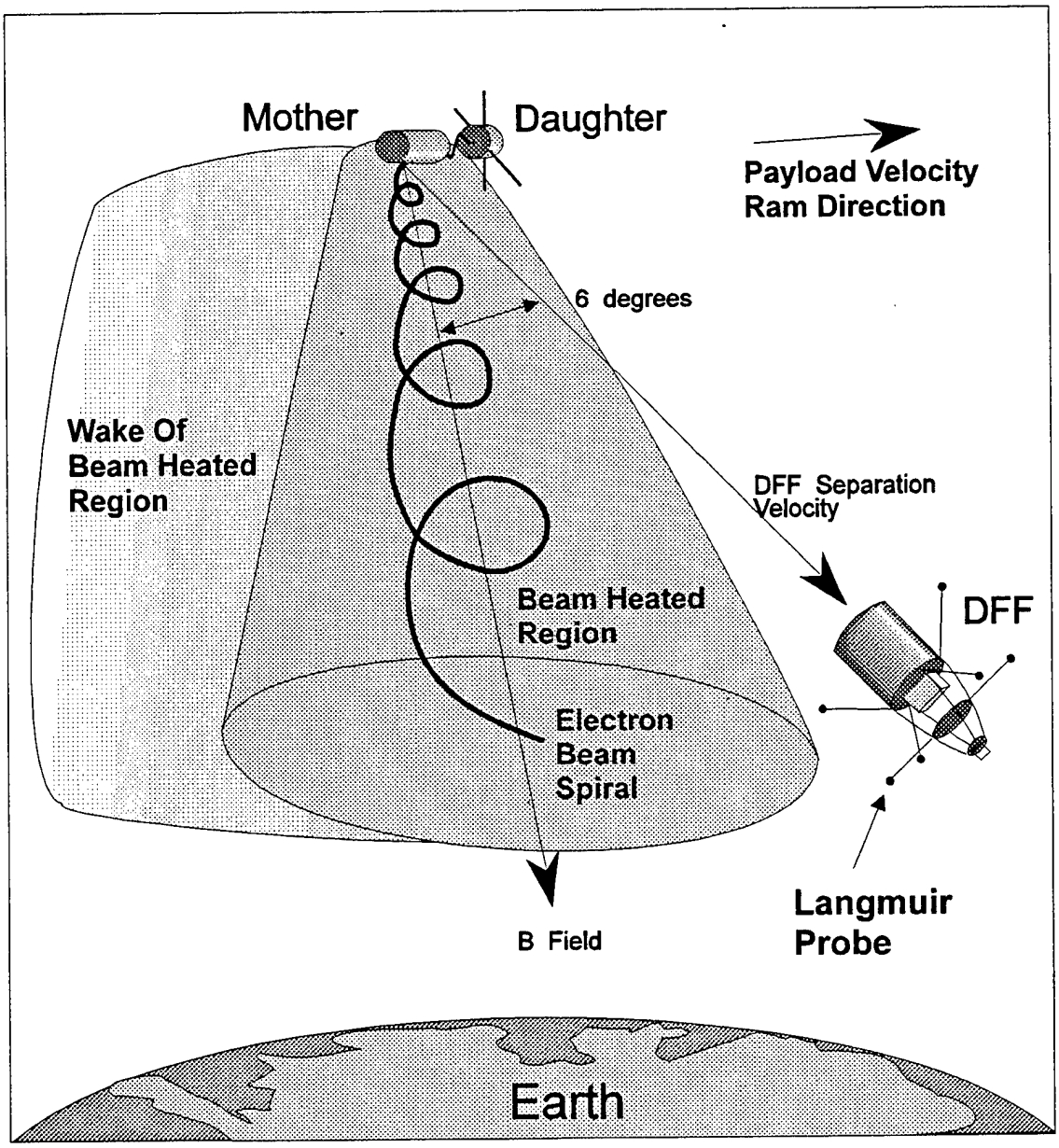

Figure 9. DFF Deployment Direction. The DFF was separated from the mother payload at an angle of six degrees from the geomagnetic field in the ram direction. The entire payload (mother, daughter and DFF) moved along the trajectory at the payload velocity (typically 1 km/s) while the DFF drifted away from the mother-daughter system at the separation velocity (5.3 m/s).

The maximum radius of the spiral occurs when the electron beam is emitted with a pitch angle to the magnetic field of 90 degrees. The radius of the spiraling electrons is called the Larmor radius r_L and is defined as[8]

[8] Chen, F. F. (1977) *Introduction to Plasma Physics*, Plenum Press, New York.

$$r_L = \frac{m v_\perp}{e B} \tag{11}$$

where $v_\perp$ is the beam electron velocity perpendicular to the geomagnetic field, and B is the geomagnetic field strength. The velocity of the beam electrons must be calculated to determine the Larmor radius. This can be done by defining temperature in units of energy[8]

$$E = \frac{1}{2} m v^2 = k T_e \tag{12}$$

Rearranging and defining temperature in terms of electron Volts (kT_e/e)

$$v = \sqrt{\frac{2e}{m} \cdot \frac{kT_e}{e}} \tag{13}$$

This gives a beam velocity of 3.2×10^7 m/s for the 3 keV electron beam. Substituting this into Eq. (11) and using a magnetic field of 0.5 G yields a maximum Larmor radius of 3.7 m.

Thus there was a column of highly energized beam electrons near the DFF during electron beam operations. In fact, previous experiments have shown that there is a heated region surrounding the beam column that is much larger than that of the Larmor radius of the beam electrons.[9] So it is expected that during the early beam operations the DFF was in the heated plasma environment surrounding the electron beam.

Electron temperatures derived from Figure 10 were over 3 eV, which is more than an order of magnitude greater than the 0.2 eV temperature characterizing the quiescent background plasma during the CHARGE-2B experiment. These observations were made during electron beam operations on the Mother early in the flight, beginning with the earliest beam current emissions 140 seconds after launch and ending near 195 seconds after launch. At the time of the last observation of elevated electron temperature, the DFF was 43 m away from the Mother in a direction perpendicular to the geomagnetic field, and 400 m away along the field.

The DFF was ejected in the plane of the system trajectory, with a 5.3 m/s relative velocity that kept it ahead of the volume occupied by the electron beam. As a result, the DFF never entered the beam wake, where heated populations are known to persist for tens of milliseconds.[10] Any observations of elevated electron temperature must therefore

---

[9] Winckler, J.R., and Erickson, K.N. (1990) Plasma heating, electric fields and plasma flow by electron beam ionospheric injection, *Adv. Space Res.*, **10**:(7)119-(7)124.

[10] Cartwright, D.G., Monson, S.J., and Kellogg, P.J. (1978) Heating of the ambient ionosphere by an artificially injected electron beam, *J. Geophys. Res.*, **83**:16-24.

indicate that the DFF was in the primary heated plasma column around the electron beam. This implies a value of 43 m for the maximum observed radial extent of the heated plasma column.

The fact that the heated plasma region extended beyond the beam electron Larmor radius calculated above is evidence for the important role that ions play in the return current system of an electron beam-emitting spacecraft.[9] Ions are drawn into the beam column by the electrostatic field of the negative space charge residing there immediately after beam turn-on. The perpendicular extent of the disturbed plasma region is expected to be on the order of the heated ion Larmor diameter. For the dominant ionic component at the altitudes of interest (namely O^+),[11] at a temperature of 3 eV, this dimension will be 40.0 m. This agrees with the observed value of 43 m for maximum radial extent of the heated plasma column.

Immersion of the DFF in a much hotter than ambient plasma had an interesting side effect. This may be seen in Figure 10, which shows the floating skin potential of the DFF in the upper panel and the applied sweep voltage to the Langmuir probe in the lower panel. In particular, we see by comparing Figure 3 to Figure 10 that while the DFF was within the heated plasma region, the Langmuir probe was no longer able to force negative excursions in the vehicle skin potential. This is because the hot plasma placed the entire vehicle at a more negative floating potential than the quiescent plasma. An ionospheric spacecraft will typically float to about 1 V negative due to the higher mobility of electrons compared to ions. However, in the presence of beam-generated, supra-thermal electrons, payloads in the Echo 3 experiment measured floating potentials of more than 4 V negative.[12] This is consistent with our CHARGE-2B observations.

In Figure 10, with the DFF at a floating potential of -4 V, only when the Langmuir probe was biased close to +5 V did it begin to go above plasma potential and force the skin below its floating potential. Other observations within the heated region near the time of Figure 10 show no tendency for the Langmuir probe to influence the skin potential, suggesting that the DFF floating potential was below -5 V at those times. The electron gun was switched off at 174.5 s. At this point the plasma began to return to the ambient state, as evidenced by the effect on the skin potential of the 3 V applied voltage step at 174.9 s. This applied voltage would have had no effect on the skin potential if the electron beam were heating the plasma, as may be seen at the 3-V points in the ramp sweep at 174.25 and 174.5 s. The electron beam was turned on again at 175.4 s and there was a jump in the DFF skin potential measurement. During the beam emission from 175.4 to 178 s the effect of the 1 Hz spin rate of the DFF can be seen in the skin potential measurements.

---

[11] Banks, P.M., and Kockarts, G. (1973) *Aeronomy, Part B*, Academic Press, New York.

[12] Arnoldy, R.L., and Winckler, J.R. (1981) The hot plasma environment and floating potentials of an electron-beam-emitting rocket in the ionosphere, *J. Geophys. Res.*, **86**:575-584.

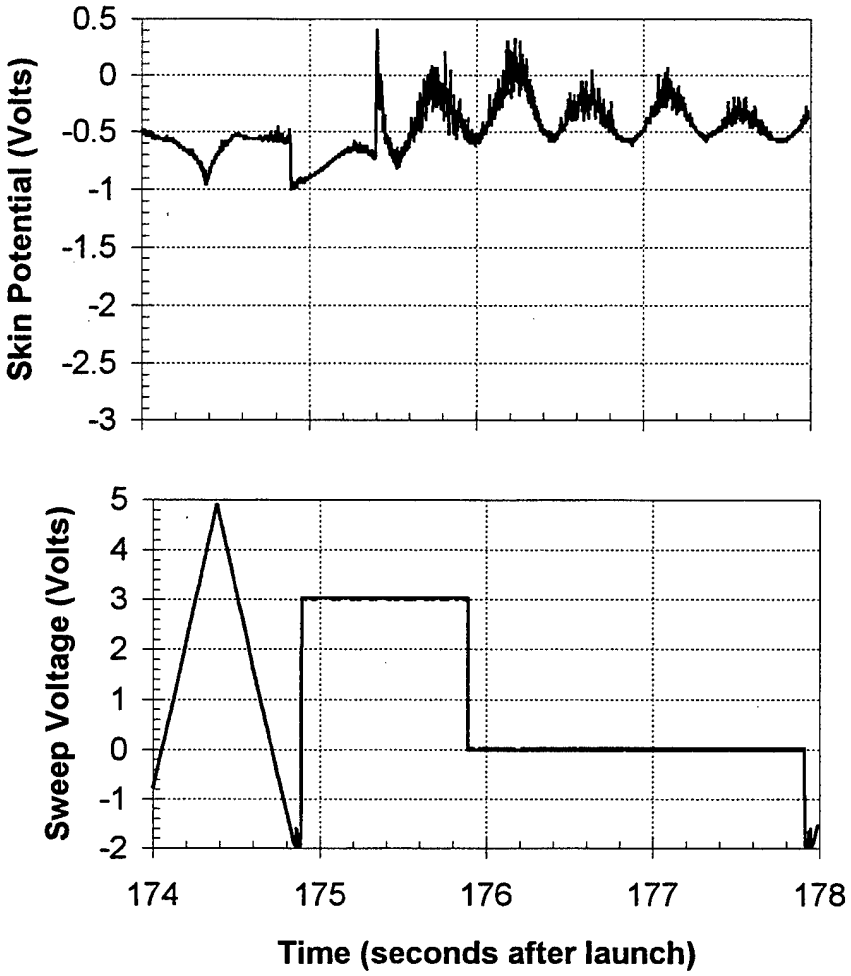

Figure 10. DFF Skin Potential While in Heated Plasma. This plot is similar to Figure 2, but is taken at 174.0 seconds after launch. Because the floating potential of the DFF skin was strongly negative while in the heated plasma, positive applied bias on the Langmuir probe grid only barely brought it to the plasma potential.

6. ELECTRON DENSITY FLUCTUATION MEASUREMENTS

The conditioned Langmuir probe current signal was sampled by telemetry at a rate fast enough to permit the observation of electrostatic ion waves characteristic of the vehicle neutralization process. The important frequency in this regime is the atomic oxygen cyclotron frequency, 47.6 Hz. However, the time domain observations reveal a very low level of density fluctuation, and in the frequency domain, no coherent emissions were found, as shown in Figure 11.

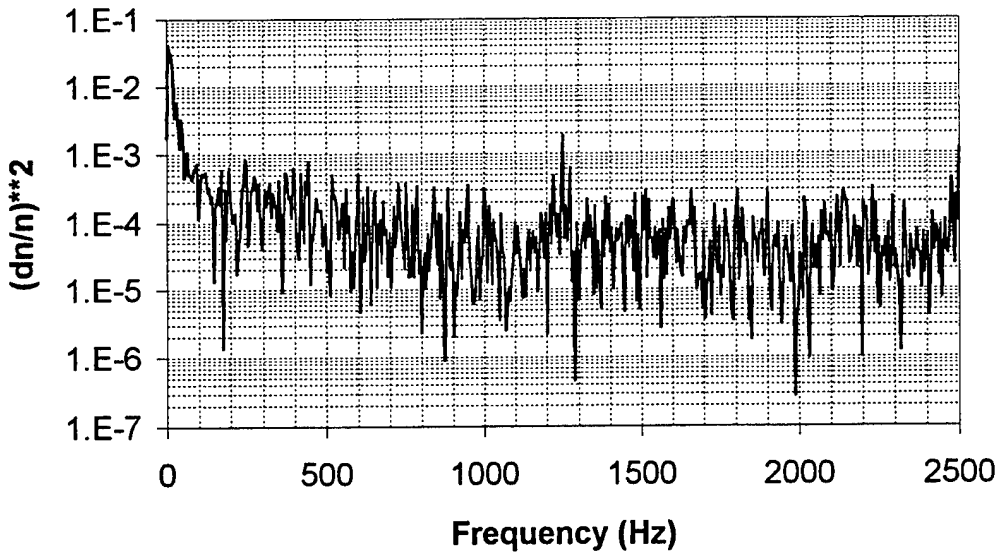

Figure 11. FFT of the Langmuir Probe Measurements When the Sweep Voltage was Held at Zero Volts 192 Seconds After Launch. Density fluctuation is plotted against frequency. The frequency resolution was 4.9 Hz. No peak is observed at the ion cyclotron frequency of 47.6 Hz.

The lack of observed fluctuations prompted concern that a subtle, instrument-related effect was limiting the bandwidth of the Langmuir probe channel below the 2500 Hz anti-aliasing filter roll off. Fortunately, the instrument response to rapid variations in collected current was amply demonstrated in the data. Figure 12 shows the calibrated Langmuir probe current during a period in the sweep when the probe bias was rapidly switched from -2V to +3V, seen at the 0 ms position on the time axis. We can determine from this plot that the output was able to slew at a minimum rate of 3.5 kV/s, determined from the slope of the line at 0 ms before applying the calibration from telemetry voltage of Eq. (2). Since the frequency bandwidth of an instrument may be expressed as[13]

$$F_{max} = \frac{S}{2\pi V_p} \tag{14}$$

where S is the slew rate, and V_p is the peak voltage, the instrument can measure a full power bandwidth (over the 5 V telemetry range) of at least 225 Hz and a small signal (< 0.5 V peak) bandwidth of at least 1.1 kHz. We therefore conclude that the lack of electron density fluctuations near the ion cyclotron frequency (47.6 Hz) at the DFF is an accurate observation, and not the result of any shortcoming of the instrument.

---

[13] Horowitz, P., and Hill, W. (1989) *The Art of Electronics*, Cambridge University Press, New York, pp 192-193.

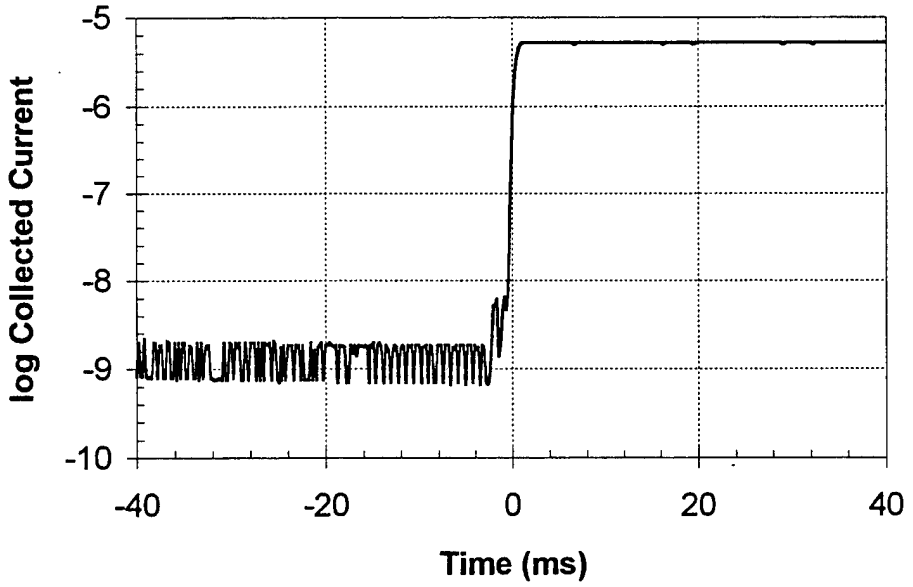

Figure 12. Langmuir Probe Step Response. The frequency response of the Langmuir probe collected current channel can be inferred from this plot of collected current versus time during a sharp transition in applied probe bias. Zero milliseconds occurs at 170.849 seconds after launch.

7. CONCLUSIONS

The DFF Langmuir probe successfully measured the local electron density and temperature throughout the flight of the CHARGE-2B sounding rocket. The altitude profile of the electron density showed unusually high values at altitudes down to 125 km. This was the result of a diffuse auroral condition at the time of the flight. Maximum observed density was 7.0×10^5 cm^{-3}. Typical background electron temperatures were in the range 0.1 - 0.2 eV. The F region peak was not observed during the flight and therefore must have been at an altitude greater than 267 km.

Elevated electron temperatures were observed while the DFF-to-Mother separation was less than 43 meters transverse to the geomagnetic field. These temperatures were as much as an order of magnitude greater than the background values. The observed extent of this heated plasma region was consistent with the predicted size of an ion-controlled return current system around the Mother and the beam column. During periods of immersion in the heated plasma, the floating potential of the DFF was as much as 5 V below the background plasma potential.

The Langmuir probe did not detect significant electron density fluctuations in the ELF band. This contrasts with the broad spectrum of strong electrostatic turbulence observed in the VLF by the DFF electric fields experiment.[14]

[14] Ernstmeyer, J., Myers, N.B., and Raitt, W.J. (1993) In-situ observations of vlf waves generated by a modulated electron beam in the ionosphere, *Adv. Space Res.*, **13**:(10)95-(10)98.

References

1. Raitt, W.J., Ernstmeyer, J., Myers, N.B., White, A.B., Sasaki, S., Oyama, K-I, Kawashima, N., Fraser-Smith, A.C., Gilchrist, B.E., and Hallinan, T.J. (1995) VLF wave experiments in space using a modulated electron beam, *J. Spacecraft and Rockets*, **32**:670-679.

2. Helliwell, R.A. (1965) *Whistlers and Related Ionospheric Phenomena*, Stanford University Press, Stanford.

3. Schriver, D., Sotnikov, V.I., Ashour-Abdalla, M., and Ernstmeyer, J., Propagation of beam-driven VLF waves from the ionosphere toward the ground, *Journal of Geophysical Research*, **100**: 3693-3702.

4. Hallinan, T.J. (1993) *Video Imaging of CHARGE IIB Auroral Streaks*, RL-TR-93-242, Final Report, Contract F19628-91-K-0035, University of Alaska, Fairbanks.

5. Ernstmeyer, J., and Donatelli, D.E. (1990) Vehicle charging and associated HF wave phenomena during electron beam emissions, *Radio Science*, **25**:263-275.

6. Boyd, R.L.F. (1968) Langmuir probes on spacecraft, in *Plasma Diagnostics*, Lochte-Holtgreven, Ed., John Wiley and Sons, New York.

7. Chen, F. F. (1965) Electric probes, in *Plasma Diagnostic Techniques*, R.H. Huddleston and S.L. Leonard, Ed., Academic Press, New York.

8. Chen, F. F. (1977) *Introduction to Plasma Physics*, Plenum Press, New York.

9. Winckler, J.R., and Erickson, K.N. (1990) Plasma heating, electric fields and plasma flow by electron beam ionospheric injection, *Adv. Space Res.*, **10:**(7)119-(7)124.

10. Cartwright, D.G., Monson, S.J., and Kellogg, P.J. (1978) Heating of the ambient ionosphere by an artificially injected electron beam, *J. Geophys. Res.*, **83**:16-24.

11. Banks, P.M., and Kockarts, G. (1973) *Aeronomy, Part B*, Academic Press, New York.

12. Arnoldy, R.L., and Winckler, J.R. (1981) The hot plasma environment and floating potentials of an electron-beam-emitting rocket in the ionosphere, *J. Geophys. Res.*, **86**:575-584.

13. Horowitz, P., and Hill, W. (1989) *The Art of Electronics*, Cambridge University Press, New York, pp 192-193.

14. Ernstmeyer, J., Myers, N.B., and Raitt, W.J. (1993) In-situ observations of VLF waves generated by a modulated electron beam in the ionosphere, *Adv. Space Res.*, **13:**(10)95-(10)98.

MISSION

OF

ROME LABORATORY

Mission. The mission of Rome Laboratory is to advance the science and technologies of command, control, communications and intelligence and to transition them into systems to meet customer needs. To achieve this, Rome Lab:

a. Conducts vigorous research, development and test programs in all applicable technologies;

b. Transitions technology to current and future systems to improve operational capability, readiness, and supportability;

c. Provides a full range of technical support to Air Force Materiel Command product centers and other Air Force organizations;

d. Promotes transfer of technology to the private sector;

e. Maintains leading edge technological expertise in the areas of surveillance, communications, command and control, intelligence, reliability science, electro-magnetic technology, photonics, signal processing, and computational science.

The thrust areas of technical competence include: Surveillance, Communications, Command and Control, Intelligence, Signal Processing, Computer Science and Technology, Electromagnetic Technology, Photonics and Reliability Sciences.